

# Magnetic Field Analysis of Wireless Power Transfer via Magnetic Resonant Coupling or Electric Vehicle

Katsumi Kesamaru \*

**Abstract** – This paper describes the magnetic field analysis of wireless power transfer via magnetic resonant coupling. The wireless power transfer system for supplying power to electric vehicle is developed. The parameters of coil transfer system are simulated by the finite element method (FEM). Therefore the coil structure of power transfer system can be accurately analyzed. This paper deals with 3kW wireless transfer system.

**Keywords:** Electric vehicle, Wireless, Power transfer, Resonant coupling, Field analysis

## 1. Introduction

A wireless power transfer system has the advantages in respect of less maintenance when the power is fed to the electric vehicle. By Kurs et al. the magnetic resonant coupling system was presented at 2007 [1]. Then the references about wireless transfer system have already been published, in which Hagiwara provides an analytical explanation of this principle by equivalent circuit [2] and Imura et al explains the principle by magnetic field analysis [3].

The wireless power transfer has already been put to practical use of charging the small sized batteries. The practical application to charging the large batteries of electric vehicles is expected.

In this paper we deal with the 3kW wireless power transfer system via magnetic resonant coupling as a home use. In this application, it is necessary to improve the efficiency of transfer system. Therefore the 3-dimensional modeling of the coupled coils is carried out in order to determine the effects of coil displacement on the transfer power.

## 2. Wireless Power Transfer System

Fig. 1 shows the wireless power transfer system via magnetic resonant coupling for charging the battery of electric vehicle. The system consists of battery, charging circuit, coils, capacitor and ac source. The primary or transmitting coil is on the ground, and the secondary or

receiving coil is on the vehicle. The structure of primary and secondary coils is the same.

In the 3kW model, the rated distance between coils is 30cm, and the resonant frequency is 250 kHz. In Table 1, the specifications of coils are shown.

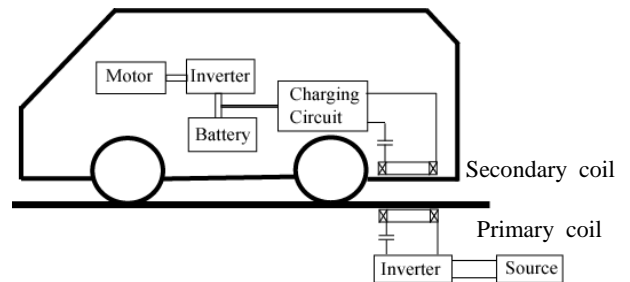


**Fig. 1.** Wireless power transfer for electric vehicle

**Table 1.** Specifications of coils

	Diameter (cm)	Cross Sec. Area(cm <sup>2</sup> )	Number of Turns	Resistance $R_c(\Omega)$
Primary Coil	30	2×2	9	0.015
Secondary Coil	30	2×2	9	0.015

## 3. Simulation of Coils System

### 3.1 Magnetic Field Analysis

Fig. 2 shows the model of coils. In order to decide the parameters of coils accurately, the 3-dimensional finite element analysis is carried out. Software JMAG-Designer is used.

Fig. 3 shows the subdivisions for 3d-FEA. The whole domain of model was divided into 47069 elements with 8470 nodes. Specified boundary condition A=0 was applied

\* Dept. of Electrical and Electronics Engineering, Kyushu University, Japan. (kesamaru@ees.kyushu-u.ac.jp)

Received 11 October 2013; Accepted 25 November 2013

on outer boundary. That is, the dirichlet condition is applied.

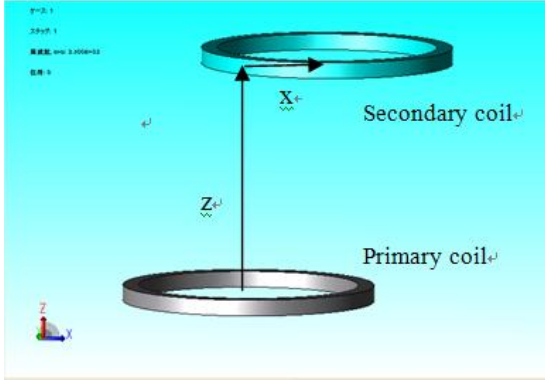


Fig. 2. 3-dimensional model of coil system

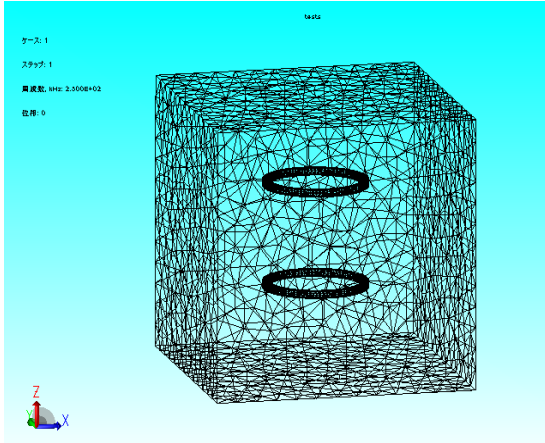


Fig. 3. subdivisions for 3D-FEA

For simplicity of FEM analysis, the following assumptions are made.

- Vector potential  $A$  and Current  $J$  changes in the sinusoidal wave in time: By this assumption, the complex approximation method can be adopted.
- The skin effect is ignored, then the current density distribution is uniform in the cross section of coils. This assumption is valid if we use the Litz wire as the coil windings.

Fig. 4 shows the mutual inductance  $M$  and the coupling coefficient  $k$  with the distance  $z$  between coils at alignment  $x=0$ . By dotted line, the case of therated distance equal to 30cm is illustrated. The mutual inductance  $M$  is  $1.27\mu\text{H}$ , and the coupling coefficient  $k$  is 0.032.

Fig. 5 shows the mutual inductance  $M$  and the coupling coefficient  $k$  with the displacement  $x$  between coils at the distance  $z=30\text{cm}$ . When the secondary coil is displaced by half pitch of diameter, the mutual inductance is reduced by 20 %.

The self inductance  $L$  is  $40\mu\text{H}$ , and then the resonant

capacitor  $C$  is  $10.13\text{nF}$ .

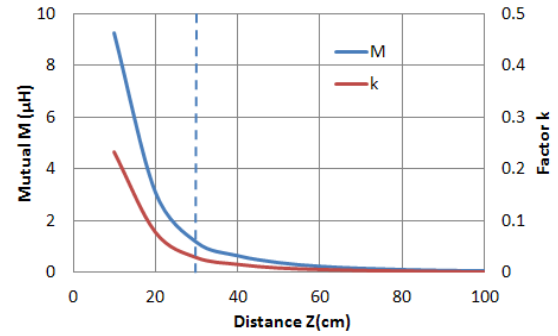


Fig. 4. Variations of  $M$  and  $k$  vs. distance  $z$  (displacement  $x=0$ )

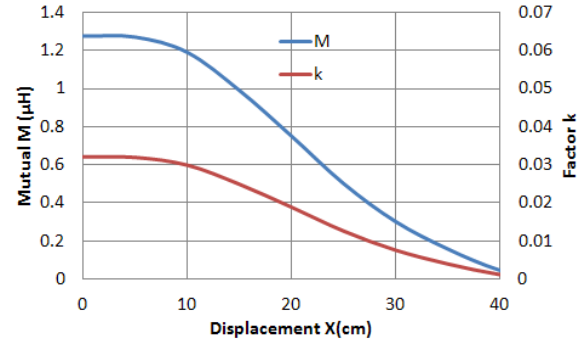


Fig. 5. Variations of  $M$  and  $k$  vs. displacement  $x$  (distance  $z=30\text{cm}$ )

### 3.2 Equivalent Circuit

On the basis of main parameters( $M, L$ ) determined above the equivalent circuit is derived, and the characteristics is analyzed. The parameters are as follows. Source Voltage  $E$  is  $70\text{V(rms)}$ , Source impedance  $R_s$  is  $0.1\Omega$ , Resonant capacitor  $C$  is  $10.13\text{nF}$ , Coil resistance  $R_c$  is  $0.015\Omega$  and self-inductance  $L$  is  $40\mu\text{H}$ .

Fig. 6 shows the equivalent circuit of the wireless power transfer system. The following matrix is derived by applying circuit theory.

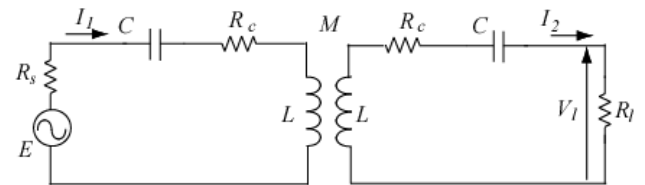


Fig. 6. Equivalent circuit of the system

$$\begin{bmatrix} Z_1 & -j\omega M \\ -j\omega M & Z_2 \end{bmatrix} \begin{bmatrix} I_1 \\ I_2 \end{bmatrix} = \begin{bmatrix} E \\ 0 \end{bmatrix} \quad (1)$$

where,

$$Z_1 = R_S + R_C + jX_{LC}, \quad Z_2 = R_l + R_C + jX_{LC},$$

$$X_{LC} = \omega L - \frac{1}{\omega C}$$

By solving the above matrix equation, the source power  $P_s$ , the load power  $P_l$ , and the efficiency  $\eta$  are obtained as follows,

$$P_s = \frac{(R_l + R_c)X_0 + X_{LC}Y_0}{X_0^2 + Y_0^2} E^2 \quad (2)$$

$$P_l = \frac{R_l \omega^2 M^2}{X_0^2 + Y_0^2} E^2 \quad (3)$$

and

$$\eta = \frac{P_l}{P_s} \quad (4)$$

where

$$X_0 = (R_S + R_C)(R_l + R_C) + \omega^2 M^2 - X_{LC}^2$$

$$Y_0 = (R_S + R_l + 2R_C)X_{LC}$$

At the resonant condition equal to  $X_{LC}=0$ ,  $P_s$ ,  $P_l$  and  $\eta$  is expressed as follows

$$P_s = \frac{R_l + R_c}{(R_l + R_c)(R_S + R_C) + \omega_0^2 M^2} E^2 \quad (5)$$

$$P_l = \frac{R_l \omega_0^2 M^2}{((R_l + R_c)(R_S + R_C) + \omega_0^2 M^2)^2} E^2 \quad (6)$$

and

$$\eta = \frac{R_l \omega_0^2 M^2}{(R_l + R_c)((R_l + R_c)(R_S + R_C) + \omega_0^2 M^2)} \quad (7)$$

where

$$\omega_0 = 2\pi f_0, \quad f_0 \text{ is the resonant frequency.}$$

From above equations, by increasing the load resistance  $R_l$ , the load power  $P_l$  increases, and the efficiency  $\eta$  decreases. In the same way, by increasing the mutual inductance  $M$ , the power  $P_l$  decreases, and the efficiency increases.

#### 4. Analytical Results

Fig. 7 shows the variations of the power  $P_s$ ,  $P_l$  and efficiency  $\eta$  with load resistance  $R_l$ . At load resistance  $3\Omega$ , the power  $P_l$  is 3.5kW, and the efficiency  $\eta$  is 0.90.

Fig. 8 shows the variations of  $P_s$ ,  $P_l$  and  $\eta$  with coil displacement  $x$ . When the secondary coil is displaced by half pitch of diameter, the power  $P_l$  increases from 3.5kW to 4.5kW, and the efficiency  $\eta$  decreases from 0.90 to 0.86. At this variation range of coil displacement a high efficiency is maintained and the deterioration is less.

Fig. 9 shows the variations of  $P_s$ ,  $P_l$  and  $\eta$  with the source frequency  $f$ . The powers  $P_s$  and  $P_l$  decrease except for the resonant frequency equal to 250 kHz. The change of efficiency  $\eta$  becomes small.

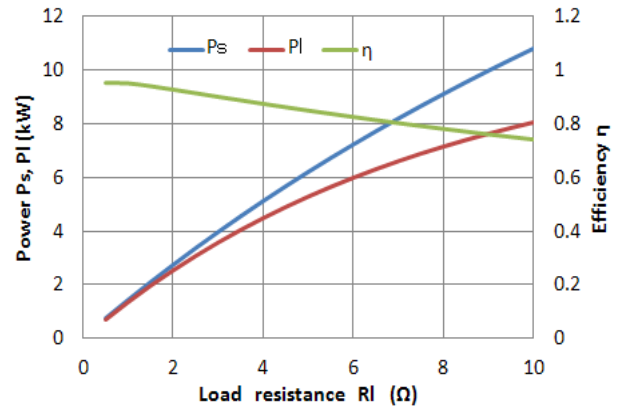


Fig. 7. Load characteristics at  $x=0$  and  $z=30\text{cm}$

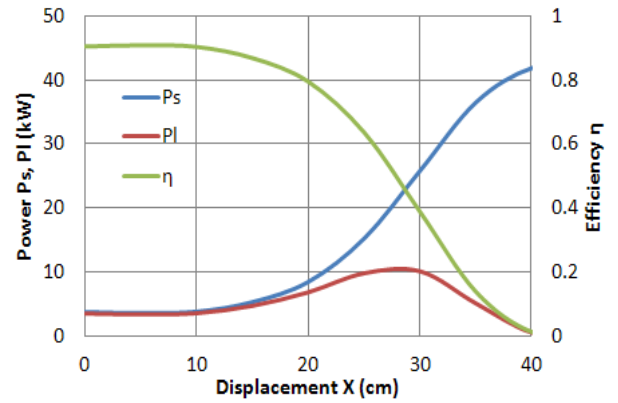


Fig. 8. Displacement characteristics at  $R_l=3\Omega$  and  $z=30\text{cm}$

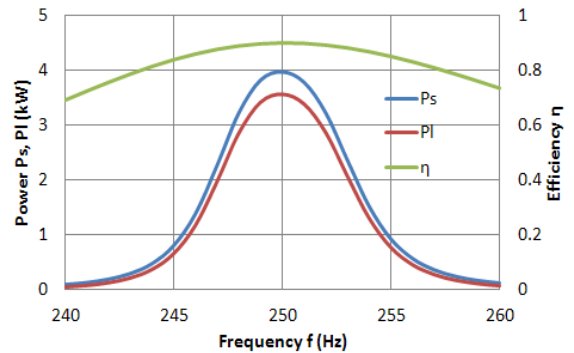


Fig. 9. Frequency characteristics at  $x=0$ ,  $z=30\text{cm}$  and  $R_l=3\Omega$

Fig. 10 shows the waveforms of voltage and current at 3.5kW. The rms value of primary current  $I_1$  is 56A. The rms value of secondary current  $I_2$  is 34A. The phase angle between  $i_1$  and  $i_2$  is about  $90^\circ$ .

Fig. 11 (a) and (b) plot the vectors of the magnetic flux density, at  $\omega t=90^\circ$  and  $\omega t=180^\circ$ , respectively. These plots are corresponding for the waveforms of Fig.10. The maximum of flux density is 0.0137T on primary coil of Fig. 11 (a).

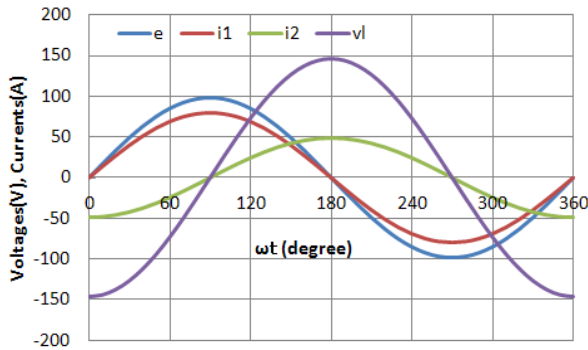
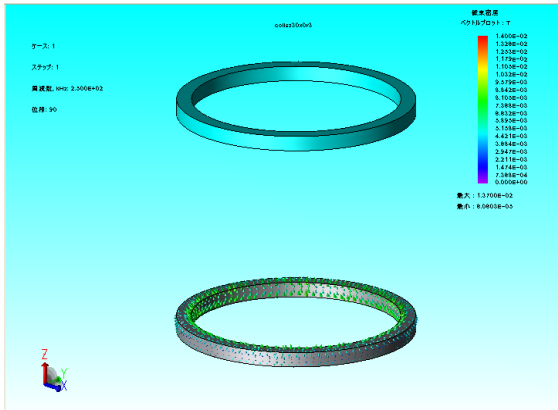
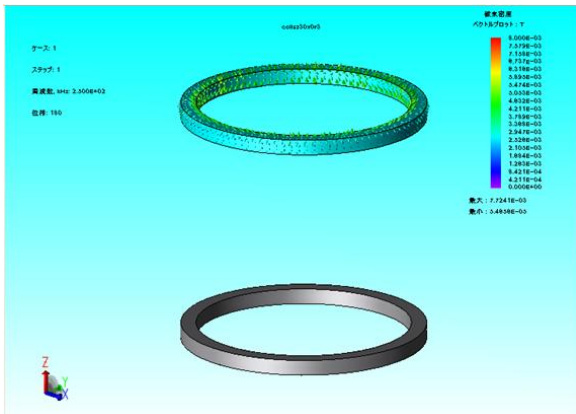


Fig. 10. Waveforms of voltages and currents at  $R_f=3\Omega$



(a)  $\omega t=90^\circ$



(b)  $\omega t=180^\circ$

Fig. 11. Vector of magnetic flux density at  $R_f=3\Omega$  ( $z=30\text{cm}$  and  $x=0$ )

## 5. Investigation of Coil Structure

The effects of geometry of coil cross section on power transfer characteristics were investigated.

Table 2 shows the specifications of coils, in which the geometry of coil cross section is flat. The cross section area is the same as that of square type coil section in shown in Table 1.

Table 2. Specification of coils (Flat type)

	Diameter (cm)	Cross Sec. Area( $\text{cm}^2$ )	Number of Turns	Resistance $R_c(\Omega)$
Primary Coil	30	$0.4 \times 10$	9	0.015
Secondary Coil	30	$0.4 \times 10$	9	0.015

Fig. 12 shows the mutual inductance  $M$  with the displacement  $x$  between coils at the distance  $z=30\text{cm}$ . Mutual inductances for Square type and Flat type are about same but in the range of 10 to 20cm, the square type is a little higher.

Fig. 13 shows the coupling factor  $k$  with the displacement  $x$  between coils at the distance  $z=30\text{cm}$ . The self inductance  $L$  of flat type coil is  $27\mu\text{H}$ . Due to small self-inductance, the factor  $k$  is larger than that of square type coil.

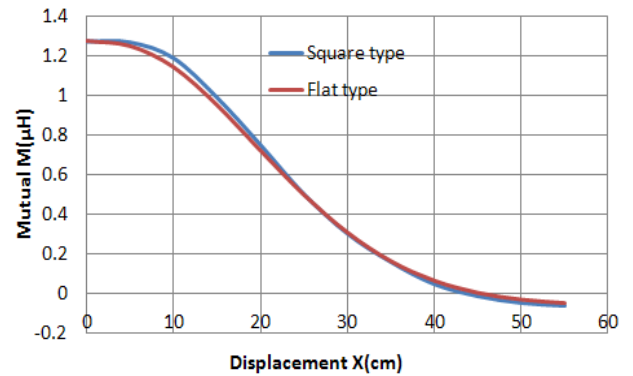


Fig. 12. Variations of  $M$  vs. displacement  $x$  ( $z=30\text{cm}$ )

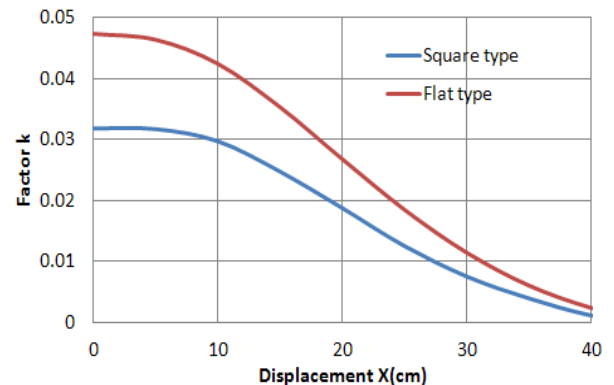


Fig. 13. Variations of  $k$  vs. displacement  $x$  ( $z=30\text{cm}$ )

Fig. 14 and 15 show the variations of load power  $P_l$  and efficiency  $\eta$  with coil displacement  $x$  at load resistance  $3\Omega$ . The differences cannot be found almost. In detail, the square type is slightly better in efficiency.

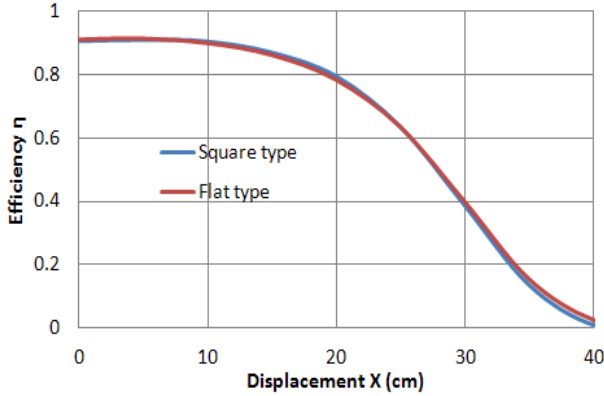


Fig. 14. Power vs. displacement at  $R_l=3\Omega$  and  $z=30\text{cm}$

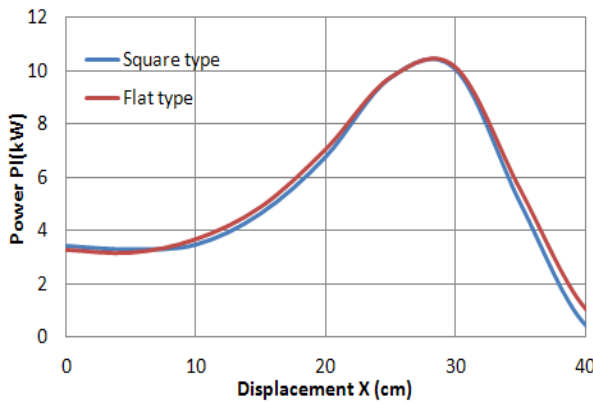


Fig. 15. Efficiency vs. displacement at  $R_l=3\Omega$  and  $z=30\text{cm}$

Fig.16 shows the vectors of the magnetic flux density at  $\omega t=180^\circ$ . The maximum of flux density is 0.0048T on secondary coil. The magnetic density is small with that of Fig.11 (b).

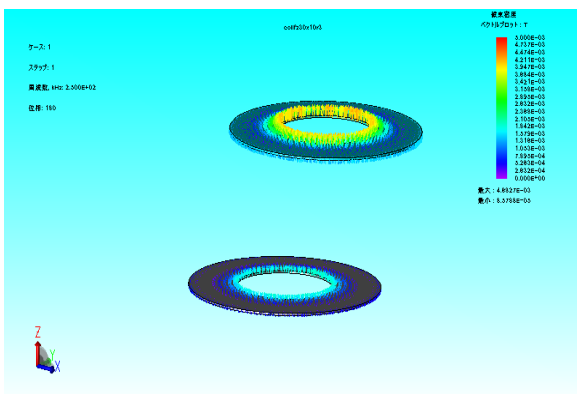


Fig. 16. Vector of magnetic flux density at  $R_l=3\Omega$  ( $z=30\text{cm}$  and  $x=10\text{cm}$ )

## 6. Conclusion

In this paper, the magnetic field analysis of wireless power transfer via magnetic resonant coupling for electric vehicle has been described.

The 3-dimensional modeling of the coupled coils is carried out in order to determine the effects of coil displacement on the transfer power.

If the secondary coil is displaced in the range of the half coil, it is confirmed that the deterioration is less.

As analytical results, this wireless power transfer system is suitable for charging electric vehicle, because the system can be transfer power wireless with high efficiency and large air gap when the vehicle are displaced by half coil pitch.

## Acknowledgements

The author thanks H. Fujibe of Kyushu University for his cooperation in conducting finite element method.

## References

- [1] A. Kurs, et. al, "Wireless power transfer via strongly coupled magnetic resonances," in *Science Express* on 7 June 2007, vol. 317, no.5834, pp.83-86, June, 2007.
- [2] N. Hagiwara, "Study on the principle of contactless electric power transfer via electromagnetic coupling," *IEEJ Transactions on IA*, vol. 131, no. 5, pp. 708-713, May, 2011.
- [3] T. Imura, Y. Hori, "Determination of limits on air gap and efficiency for wireless power transfer via magnetic resonant coupling by using equivalent circuit," *IEEJ Transactions on IA*, vol. 130, no.10, pp. 1169-1174, October, 2010



**Katsumi Kesamaru** received M.E and Dr. Eng. degrees from Kyushu University, 1974 and 1988, respectively. His research interests are emerging electric vehicle, wind energy systems and PM machines.